Vehicle-to-Vehicle VLC Based on PSD Sensor: System Modeling and Effects of Multipath in Unfavorable Situations

Fatima Zahra Raissouni, Álvaro De-La-Llana-Calvo, José-Luis Lázaro-Galilea, Alfredo Gardel-Vicente, and Abdeljabbar Cherkaoui

***Abstract*—Vehicular communication-based visible light presents an excellent solution to ensure road safety and transportation efficiency in critical environments like tunnels, underground garages, or covered parking lots where traditionally RF solutions cannot provide an efficient communication. In this article, we propose a new multipath channel model for vehicle-to-vehicle (V2V)-visible light communication (VLC) in unfavorable situations like in tunnels by using a position-sensitive detector (PSD) sensor. The performance of the derived channel model is evaluated using statistical measures based on numerical simulations in terms of channel impulse response (CIR), channel dc gain, and root-mean-square delay spread (RMS-DS) to quantify the effects of multipath propagation. Monte Carlo simulation is also used to explore the statistical model obtained for different transmission scenarios. Additionally, we evaluate the influence of various model parameters, such as road width and intervehicular distance, on the performance of the V2V channel. The main results are compared with typical Lambertian reflector model to confirm the validity of the proposed model.**

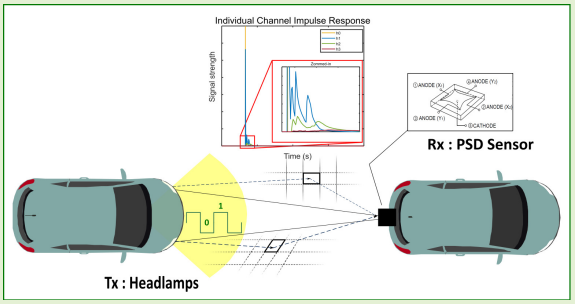

***Index Terms*—Intelligent transportation systems, multipath, position-sensitive detector (PSD) sensor, vehicle-to-vehicle (V2V), visible light communications (VLCs).**

I. Introduction

TRANSPORT systems (TS) can benefit enormously from the integration of information and communication technologies (ICTs) in vehicles and road infrastructures. One of the key objectives and benefits is to significantly enhance road safety while improving driver and passenger comfort. Driven by advanced communication solutions, these systems are a key step toward the evolution of more efficient and sustainable transport networks.

At the dawn of this new urban transport revolution, vehicle-to-vehicle (V2V) communication is positioned as one of the major innovations in TS [1]. By enabling vehicles to autonomously exchange information with each other in real-time, V2V technology represents a fundamental transformation in road mobility, going beyond improvements in comfort and safety. This interconnection, resulting from the advanced integration of modern technologies, enables unprecedented coordination, reducing accidents and making traffic flow more smoothly. This is how V2V communication is emerging as the pillar of future urban mobility, transforming every vehicle into a collaborative participant in the road network.

For V2V communications, two main technologies are currently used worldwide: Dedicated short-range communication (DSRC), which is dominated by the USA and uses the IEEE 802.11p protocol [2], and cellular V2V communication (C-V2X) [3], which uses cellular networks and can support longer ranges and higher data rates.

However, radio frequency (RF) communication is showing its limitations, particularly in specific environments such as

Manuscript received 28 February 2024; revised 20 March 2024; accepted 20 March 2024. Date of publication 1 April 2024; date of current version 15 May 2024. This work was supported in part by The GEINTRA Research Group: Electronic Engineering Applied to Intelligent Spaces and Transport Group, in part by the Ministerio de Ciencia e Innovación (MCIN)/Agencia Estatal de Investigación(AEI)/10.13039/501100011033 through REd for Indoor and Outdoor Constrained Positioning and Navigation and Its Applications (REPNIN++) under Grant RED2022-134355-T, and in part by the Community of Madrid-University of Alcala through the Project Development of Light Sources for Joint Emergency and Localization Applications (LUZEMER) under Grant PIUAH23/IA-038. The associate editor coordinating the review of this article and approving it for publication was Dr. Ing. Tai Fei. *(Corresponding author: Fatima Zahra Raissouni.)*

Fatima Zahra Raissouni is with the Department of Electronics, Escuela Politécnica Superior, University of Alcala, Alcala de Henares, 28801 Madrid, Spain, and also with the Laboratory of Innovative Technologies, National School of Applied Sciences, Abdelmalek Essaâdi University, Tangier 90060, Morocco (e-mail: fatima.raissouni@edu.uah.es).

Álvaro De-La-Llana-Calvo, José-Luis Lázaro-Galilea, and Alfredo Gardel-Vicente are with the Department of Electronics, Escuela Politécnica Superior, University of Alcala, Alcala de Henares, 28801 Madrid, Spain (e-mail: alvaro.llana@uah.es; josel.lazaro@uah.es; alfredo.gardel@uah.es).

Abdeljabbar Cherkaoui is with the Laboratory of Innovative Technologies, National School of Applied Sciences, Abdelmalek Essaâdi University, Tangier 90060, Morocco (e-mail: abcherkaoui@uae.ac.ma).

Digital Object Identifier 10.1109/JSEN.2024.3381633

road tunnels. These constraints have prompted researchers to consider alternatives, among which visible light communication (VLC) looks promising, offering greater reliability in confined spaces than RF. Moreover, VLC has the advantage of using an unlicensed optical spectrum ranging from 400 to 700 nm, and is both economical, green, and immune to electromagnetic interference.

Although this technology represents a promising enabling solution for vehicular communications in vehicular ad hoc networks (VANETs) and 6G [4], further studies are required, in particular, to analyze its behavior in complex scenarios and determine its optimal parameters. It is also essential to identify the elements that could disrupt the VLC channel in a tunnel passage. It is important to emphasize that V2V communication plays a vital role in transmitting real-time alerts and information among road users.

Moreover, the standardization of VLC under IEEE 802.11.7 [5] serves as evidence of its promising capabilities. Within this standard, PHY I is tailored for outdoor, long-distance, and low-data-transfer applications, including V2V and infrastructure-to-vehicle (I2V) communication.

Nevertheless, in-depth studies are required to optimize its deployment, notably to assess its behavior in different scenarios and to understand the external factors influencing the VLC channel in closed environments.

The structure of the article is as follows: In Section II, we provide background information and review related works. Section III delineates the proposed system model, focusing on evaluating communication behavior. Section IV elaborates on the primary features of vehicular VLC channels. Section V unveils the simulation results and engages in discussion. Section VI presents the conclusions drawn from the study.

II. Background

Underground structures and semiconfined environments such as tunnels offer unique signal transmission characteristics, contrasting sharply with open environments [6]. Understanding V2V communications in these singular environments is crucial for modern, innovative transportation systems, in order to optimize the integration of tomorrow's safety applications, based on wireless communication.

Before exploring the background of related works on communication via VLC, it is essential to set the foundations of our understanding by first addressing RF. As the foundation of wireless communications, RF has been the focus of numerous studies and research works, including in the context of closed environments, and more specifically vehicular communication inside road-tunnels. For example, study [6] delved into V2V radio channel measurements, focusing on the singular context of a tunnel. Key parameters such as root-mean-square delay spread (RMS-DS), Doppler spread, and various other factors influencing transmission quality were investigated.

By extending this perspective, the research [7] addressed questions about how the physical dimensions of the tunnel, such as its width and height, can influence the intensity of the reflected rays. Hence, it consequently became clear that the geometric structure of the tunnel plays a main role in the dominance of reflections. Additionally, the study [8] presents a novel approach with its development of a 3-D V2V multiple input multiple output (MIMO) channel model specifically designed for a rectangular tunnel environment.

It is important to note that, despite RF predominance, this technology presents several challenges, particularly in terms of packet reception rates, especially under saturated traffic conditions [9] which pave the way for the exploration of alternative solutions. VLC technologies, with their ability to minimize interference with existing RF systems and their potential as complements to these systems, appear to be a viable alternative. Further, for position-sensitive detector (PSD)-based systems, if appropriate modulation techniques are used, it is able to distinguish the emitters in the system with little or no interference [10].

Previous research confirms the relative stability of the VLC vehicular channel [11], demonstrating a high probability of maintaining considerable coherence time with an approximate 90% probability of achieving a coherence time of a few hundred milliseconds in urban environments [12]. Moreover, an empirical investigation conducted by [9] on V2V communication via VLC revealed the criticality of the angle and distance between transmitter and receiver to ensure optimal signal reception. The reduced latency in light transmission makes V2V-VLC an effective means of transmitting safety-related information [13]. To date, several channel models have been proposed for V2V VLC communication considering different propagation environments. There are multiple works that include empirical and theoretical studies that consider stochastic and/or deterministic channel models. In works [14], [15], a geometry-based channel model for V2V VLC was presented. This model captures both line-of-sight (LOS) and non-LOS (NLOS) links, while considering the dynamic nature of vehicles. In addition, the influence of weather conditions is also considered. The model presented in [16] is distinguished by its focus on reflections from the road surface, relying on a geometric approach to capture the LOS and single bound (SB) components. It should be noted, however, that this model is limited to direct reflections from the road surface, excluding other potential interactions with the environment. In addition, other works, such as [17], [18], have focused on V2V-VLC system performance measures. These studies offer concrete measures to characterize the link, and they highlight the influence of various external agents on VLC communication in outdoor environments. Bidirectional communications are also studied for V2V-VLC systems [19] enabling full-duplex interaction between vehicles. An analysis of the system's performance, using real motorcycle headlights and taillights, was presented.

However, there are other relevant environments, such as parking lots and tunnels, which require appropriate studies to determine the predominant channel characteristics. Identifying these key features is crucial to improving the accuracy and simplicity of models, especially when it comes to complementing more general models. Specifically in tunnels, multiple reflections are a predominant propagation condition.

The application of VLC in tunnels and underground environments has already been proposed for positioning purposes [20], [21], given the limitations of global positioning systems

(GPS) in terms of accuracy. In closed environments such as mines, GPS is often inaccurate and discontinuous due to interference from signals coming from structures such as ceilings and walls. In addition, due to the presence of potentially explosive gases and unfavorable propagation conditions, RF communication technology is not suitable. In the same context, a VLC channel model for underground mining (UM-VLC) was proposed in [22]. This model includes crucial factors that significantly impact the performance of VLC in underground mine environments. Nevertheless, the use of VLC for communication purposes in tunnel environments has not been deeply studied nor implemented yet. A preliminary study of I2V channels [23] for tunnels [24] are proposed, the authors introduce a Monte Carlo ray-tracing simulation to analyze the impulse response of a vehicular VLC system proposed to be installed into a tunnel. The effect of road reflectance is considered but a fixed reflectance value is assumed for simplicity. However, this approach is not optimal for the light spectrum, where a wavelength-dependent reflectance should be considered for a realistic model.

In summary, this literature review depicts that the channel model assumed by several authors uses simplified channel modeling approaches for both confined and outdoor vehicular VLC (VVLC) environments. In a vehicular environment, the multipath phenomenon becomes more pronounced due to the reflection off diverse surfaces (vehicles, buildings, and ground), as well as the changing lighting conditions further complicate this effect. Current models, based on Lambertian reflections or assume fixed values, may be unable to capture the complexity of these light interactions in the vehicular environment.

In contrast to the existing channel models V2V-VLC, discussed above and in the literature, instead of opting for a simplified approach, we drew inspiration from the approach presented in [25], [26], and [27], which adopts a discrete modeling process bases on non-Lambertian reflection model. Although this method was originally developed for indoor visible light positioning (VLP) systems, it offers considerable advantages for V2V sensor VLC proposed herein. By partitioning the environment, it enables more accurate analysis of multipath channels, capturing the complexity of unfavorable situations such as confined environment (tunnels).

In addition, to the best of the author's knowledge, this is the first deployment of a V2V-VLC system based on PSD. However, existing research still exhibits the following shortcomings.

1) Most studies of complex scenarios focus on open-air environments. However, the importance of closed environments, which represent one of the most unfavorable situations, already discussed, seems to have been neglected. In particular, in tunnels and other confined spaces has not on V2V modeling based on VLC addresses reflections based on the standard Lambertian model, which does not accurately represent reality.
2) From this perspective, this article proposes an analysis of a PSD-based sensor for V2V VLC and a novel model for the reflection of optical signals on different surfaces.
3) A discretized methodology is adopted to model the surrounding surface. This approach enables us to obtain optical channel impulse responses (CIRs) for the V2V scenario under analysis, considering various scenarios.
4) The signal dispersion due to multipath effects is realistically bounded, since a channel model very close to the real behavior is used.

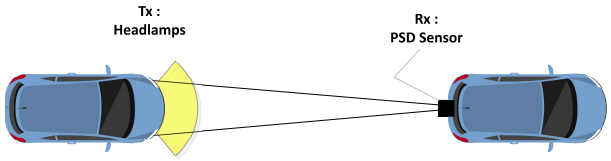

Fig. 1. V2V system model.

III. System Model

An example scenario for our proposed V2V-VLC channel model is presented in Fig. 1. We have considered a V2V-based system where the headlamps in the front of the vehicles represent the transmitters and the PSD sensor represent the receiver, initially located at the middle of the rear of the ahead vehicle. A bidirectional device could be installed independent of the illumination lights for VLC communication that could use visible or infrared signal.

Receiver Model: As mentioned above, we use a PSD as a receiver. Fig. 2 shows the electrical diagram of this sensor, illustrating a 2-D pin-cushion model. The PSD is a unique sensor consisting of four anodes and a common cathode, as shown in Fig. 2(a). In addition, Fig. 2(b) provides an illustration of the sensor when equipped with a lens.

Where (x_i, y_i) represent the impact points on the PSD sensor, f is the focal length, (X_i, Y_i, Z_i) are the points in the transmitters in the environment, and $(\theta_{xi}, \theta_{yi})$ are the angles of arrival (components of AoA), i represents each emitter. The PSD sensor presents a fast-processing alternative that offers a series of features over conventional cameras, including fast response time, good positioning accuracy, and simple signal conditioning circuitry [28]. However, it also has disadvantages such as its bandwidth is less than that of photodiodes (PDs) or photodiode arrays.

The PSD surface is 9×9 mm^2, larger than conventional PDs. This enables to capture a greater amount of light, resulting in a stronger and more reliable signal (as it can be seen in (1) -Ar-), and therefore, it will have a higher SNR. On the other hand, this makes it possible to have the same field of view (FoV) with commercial lenses of larger focal length, which makes it easier to have lenses of larger surface area and collect more energy (there are no lenses of large surface area and small focal length, for example, there are no lenses of 8 mm focal and 1-in diameter).

Fig. 3 shows the influence of focal length on FOV (coverage area).

One of the important reasons for using the PSD sensor is that, in the work that is starting to be developed, the analysis of the signal obtained by each of the PSD anodes will allow us to

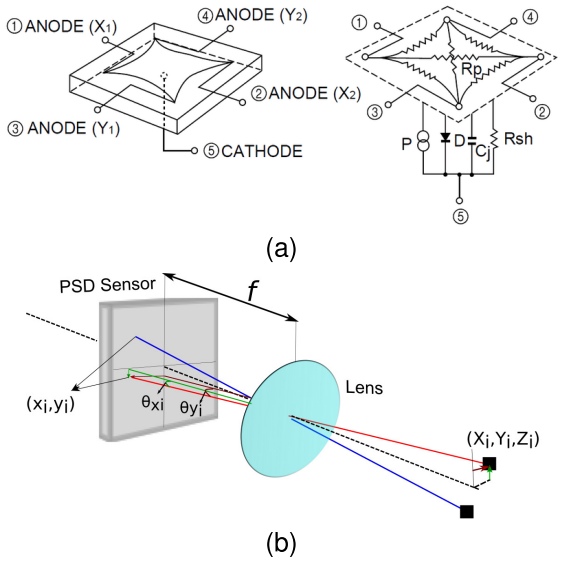

Fig. 2. Representation of the receiver system. (a) Equivalent circuit of the PSD pin-cushion (image courtesy of Hamamatsu, obtained from the PSD technical information). (b) PSD attached to a lens.

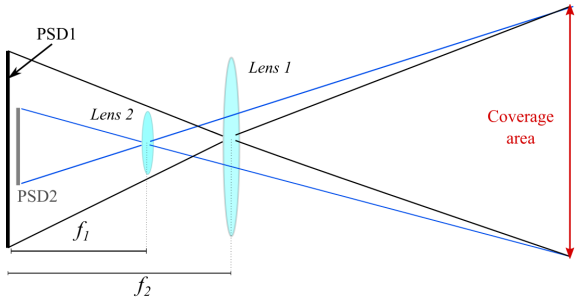

Fig. 3. Illustration of the influence of focal length on coverage area.

provide additional and accurate information about the distance and orientation of the vehicles which are critical parameters in V2V communications for safety and navigation purposes. This is essential in the vehicular context, providing a better understanding of the dynamic environment and improving the performance of the system. Another important reason is the ability to mitigate multipath effects to determine distance and orientation, as can be seen in [27].

A. Geometrical Tunnel Propagation Model

The aim of our study is to quantify the effect of multipath for V2V-VLC inside a tunnel using the proposed model and sensor. The geometrical propagation model for the V2V system inside a rectangular-shaped tunnel is shown in Fig. 4.

In this example, both the transmitter (Tx) and the receiver (Rx) vehicles are inside the tunnel and are driving in the same direction. As already mentioned, we have opted to use a recursive model proposed by our research group in [26], which aims to discretize the environment under study, where the CIR results from a countless multipath signal due to light reflections in the environment.

To accurately quantify multipath effects, it is essential to first discretize the surfaces that are the root cause of this phenomenon [25]. In a specific situation with certain parameters,

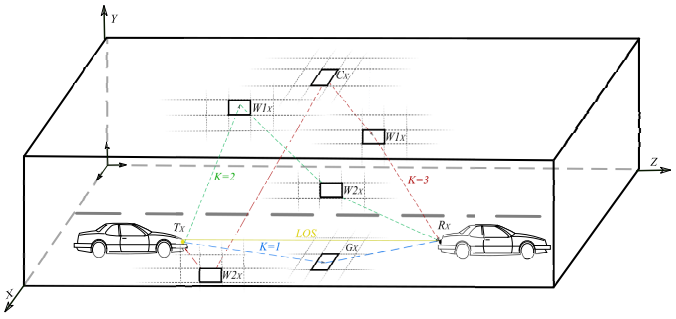

Fig. 4. Proposed V2V channel model in a tunnel environment.

the tunnel walls, road, and ceiling can be divided into a cellular grid. We then determine the signal strength in every cell based on the energy emitted by the transmitter.

For modeling reflections, each cell acts as an individual emitter, transmitting signals to adjacent cells from its midpoint according to a defined reflection pattern (both specular and diffuse).

This procedure is performed until the third rebound, when the energy becomes minimized. Every reflected signal has associated strength and phase characteristics, which guide the computation of the impulse response.

In addition, Fig. 4 illustrates three examples of multipath situations, showing third-order bounces before reaching the detector. Each path originates from the emitter, bounces off one random cell to the next, and continues this pattern until the kth reflection leads it to the detector. Cells are designated according to the type of surface they represent. For example, *Gx* refers to the cell corresponding to the ground, *w1x* and *w2x* are associated with the two respective walls, and *Cx* indicates a ceiling cell.

It is worth noting that in this article, the Lambertian model was applied exclusively to analyze light reflections in vehicular communication environments, and not for emitted light propagation itself. Our conclusion that the Lambertian model is not appropriate was specifically related to these reflections and not to light propagation in general. For the propagation model, in line with ECE R112 regulations [29], our study considers the characteristics of low-beam headlights. These are particularly relevant in tunnel environments due to their design to minimize glare and provide adequate road illumination, crucial factors at the distances we analyze (15, 25, and 35 m).

B. V2V Line of Sight Model

To model the V2V link, in an ideal channel, the received LOS signal strength P_{RT} corresponds to the energy from the transmitter defined by the given equation

$$P_{RT} = I(\omega)\frac{1}{D_{RT}^2}F(\gamma)R(\gamma)A_r = E(\omega)F(\gamma)R(\gamma)A_r. \quad (1)$$

Here, D_{RT} is the distance between the transmitter and receiver (intervehicular distance). $I(\omega)$ represent the energy output function of the transmitter can represent a generic function, and $E(\omega)$ denotes the energy per surface unit generated by the transmitter at the location of the detector. $R(\gamma)$ is

the receiver response (which includes the gain of possible concentrators and its response), and A_r is the active area of the receiver and $F(\gamma)$ is the transmission function of a potential filter placed on the receiver. If we assume that the emitter follows a Lambert model, $I(\omega)$ can be represented as:

$$I(\omega) = \frac{n+1}{2\pi} P_T \cos^n(\omega). \tag{2}$$

Here, n is the index number of the radiation lobe, P_T is the signal strength of the transmitter, and ω is the angle at which the radiant intensity emitted is assessed relative to the axial axis of the transmitter. The index n is given by the expression

$$n = -\frac{\ln(2)}{\ln\left(\cos\left(\varphi_{1/2}\right)\right)} \tag{3}$$

where $\varphi_{1/2}$ is the angle at which the signal strength is half the signal strength at 0°. The detector response relative to its axial axis, considering a thin lens, can be written as

$$R(\gamma) = \cos(\gamma)\text{rect}\left(\frac{\gamma}{\text{FoV}}\right). \tag{4}$$

If it is not possible to consider a thin lens, the $\cos(\gamma)$ must be replaced by a function $f(\gamma)$. The rectangular function is defined as

$$\text{rect}(x) = \begin{cases} 1, & \text{for } |x| \leq 1 \\ 0, & \text{for } |x| > 1 \end{cases} \tag{5}$$

where FOV is the maximum angle of arrival at which the receiver is capable of receiving. Thus, for a case that takes these last two considerations into account, without filters or thick lenses, according to (1), the received signal strength (RSS) can be expressed as

$$P_{RT} = \frac{n+1}{2\pi} P_T \cos^n(\omega) \frac{1}{D_{RT}^2} \cos(\gamma)\text{rect}\left(\frac{\gamma}{\text{FoV}}\right) A_r. \tag{6}$$

If we assume that r_T and r_R are the coordinates where the transmitter and receiver are located, respectively, whose orientations are given by the normal vectors $\vec{n}_T$ and $\vec{n}_R$, we can calculate the angles ω and γ, as well as the distance D_{RT}, as follows:

$$\omega = \arccos\left(\frac{\vec{n}_T \cdot (\mathbf{r}_R - \mathbf{r}_T)}{|\vec{n}_T||(\mathbf{r}_R - \mathbf{r}_T)|}\right) \tag{7}$$

$$\gamma = \arccos\left(\frac{\vec{n}_R \cdot (\mathbf{r}_R - \mathbf{r}_T)}{|\vec{n}_R||(\mathbf{r}_R - \mathbf{r}_T)|}\right) \tag{8}$$

$$D_{RT} = |\mathbf{r}_R - \mathbf{r}_T|. \tag{9}$$

C. Characterization of Multipath Propagation

In our proposed model, we use a non-Lambertian model to simulate multipath propagation, because Lambertian is unrealistic as a model for reflection on most situations. Our model is composed of two components:

Diffuse component, that depicts behaviors using a wide emission pattern, aligned with the normal of the reflecting surface.

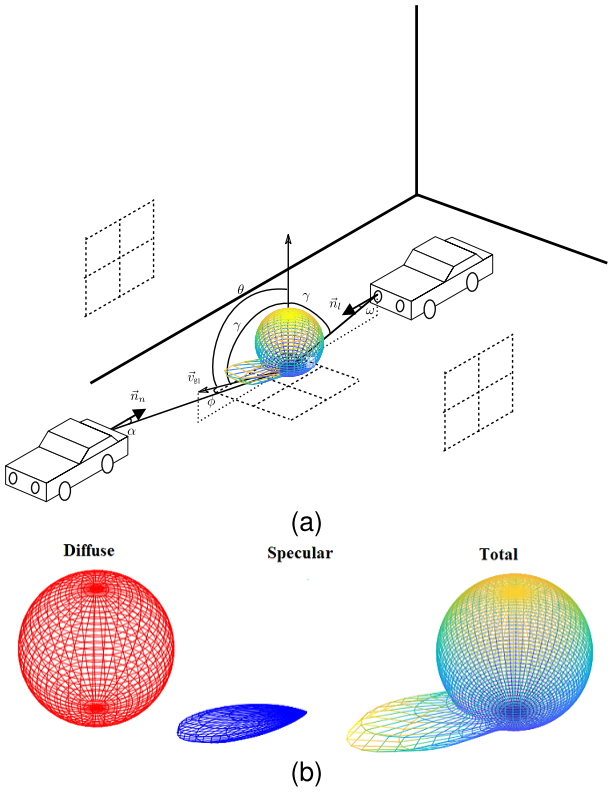

Fig. 5. Reflection model. (a) Visual representation of signal strength from reflectors. (b) Reflection components.

Specular component, shown with a more focused emission pattern, directed according to the trajectory of the beam with the highest irradiance [see Fig. 5(b)].

It should be considered that the reflection model we propose is influenced by the angle of arrival of the signal. To determine this angle necessary for the model, we first need to calculate the strength of the signal received in a cell x from a given reflection. In Fig. 5(a), we present a simplified reflection model from the ground to illustrate our approach. Imagine that Vehicle 1 is the actual transmitter.

In our scenario, this could be a random cell in the environment that receives the signal. This signal is then reflected to cell x, which in our example, represents the ground, the total reflection is depicted by shades ranging from blue to yellow. Fig. 5(b) illustrates the different reflection components: the diffuse component is symbolized by a sphere, the specular component has a blue shading, and the total reflection is the combination of both components.

As a result, the following formula represents the signal intensity that element n received as a result of element l signal strength being reflected in g (ground):

$$P_{ngl} = \left[p_d(\gamma,\theta) + p_s(\gamma,\phi)\right] S\cos(\alpha) \frac{1}{d_{ng}^2} P_{gl}\beta\text{rect}\left(\frac{\alpha}{\text{FoV}}\right). \tag{10}$$

Here, S is the area of the cells, P_{gl} is the RSS in element g from the reflection in l. The terms P_d and P_s are the diffuse

and specular components of the reflection model according to

$$p_d(\gamma,\theta) = (1-u_{as}\cos^{v_{as}}(\gamma)) \cdot \left(\frac{u_{nd}\cos^{v_{nd}}(\gamma)+1}{2\pi}\right)\cos^{u_{nd}\cos^{v_{nd}}(\gamma)}(\theta) \quad (11)$$

$$p_s(\gamma,\phi) = u_{as}\cos^{v_{as}}(\gamma) \cdot \left(\frac{u_{ns}\cos^{v_{ns}}(\gamma)+1}{2\pi}\right)\cos^{u_{ns}\cos^{v_{ns}}(\gamma)}(\phi). \quad (12)$$

α is the angle between vectors $\vec{n}_n$, and $(\mathbf{r}_g - \mathbf{r}_n)$ and is calculated as

$$\alpha = \arccos\left(\frac{\vec{n}_n \cdot (\mathbf{r}_g - \mathbf{r}_n)}{|\vec{n}_n||(\mathbf{r}_g - \mathbf{r}_n)|}\right). \quad (13)$$

d_{ng} is the distance between the element g and the element n

$$d_{ng} = |\mathbf{r}_n - \mathbf{r}_g|. \quad (14)$$

γ is the angle between the vectors $\vec{n}_g$ and $(\mathbf{r}_l - \mathbf{r}_g)$ and is calculated as

$$\gamma = \arccos\left(\frac{\vec{n}_g \cdot (\mathbf{r}_l - \mathbf{r}_g)}{|\vec{n}_g||(\mathbf{r}_l - \mathbf{r}_g)|}\right). \quad (15)$$

θ is the angle between the vectors $\vec{n}_g$ and $(\mathbf{r}_n - \mathbf{r}_g)$ and is calculated as

$$\theta = \arccos\left(\frac{\vec{n}_g \cdot (\mathbf{r}_n - \mathbf{r}_g)}{|\vec{n}_g||(\mathbf{r}_n - \mathbf{r}_g)|}\right). \quad (16)$$

φ is the angle between the vectors $(\mathbf{r}_n - \mathbf{r}_g)$ and $\vec{v}_{gl}$, where the latter is the maximum irradiance vector that can be calculated from the Householder transformation according to

$$\vec{v}_{gl} = \mathbf{H}(\mathbf{r}_g - \mathbf{r}_l) \quad (17)$$

where $\mathbf{H}$ is the Householder matrix which is defined from the normal of the reflection plane (in this case, $\vec{n}_m$), as

$$\mathbf{H} = \mathbf{I} - \frac{2\vec{n}_g\vec{n}_g^T}{\vec{n}_g^T\vec{n}_g}. \quad (18)$$

Therefore, the angle ϕ is obtained from the expression

$$\varphi = \arccos\left(\frac{\vec{v}_{gl} \cdot (\mathbf{r}_n - \mathbf{r}_g)}{|\vec{v}_{gl}||(\mathbf{r}_n - \mathbf{r}_g)|}\right). \quad (19)$$

The parameters $\vec{u}_{as}$, $\vec{v}_{as}$, $\vec{u}_{nd}$, $\vec{v}_{nd}$, $\vec{u}_{ns}$, $\vec{v}_{ns}$, and β are the parameters that characterize the material of element m defined in [25].

IV. VVLC Channel Characteristics

In this section, we will investigate the performance of the proposed V2V-VLC model, we consider different performance metrics such as CIR, channel dc gain, and RMS-DS.

A. Channel Impulse Response

The impulse response due to multipath is given by $h(t)$ and is expressed by

$$h(t) = \sum_{k=0}^{K} h_{(k)}(t) \quad (20)$$

where $h_{(k)}(t)$ is the impulse response of the k rebound and K is the number of rebounds to consider. In other words, $k = 0$ is the LOS path, $k = 1$ is the impulse response of the sum of all signals reaching the detector after a single bounce, $k = 2$ is the impulse response of the sum of all signals reaching the detector after a second bounce, and so on successively until the reflection K. The higher the K, the closer to reality, but the computational load for calculation will also rise. In our model, we used a number of reflections up to three ($K = 3$). Two functions must be used to obtain each $h_{(k)}(t)$. First, to calculate the impulse response from the source element to the receiver element for each cell in the environment, the following function is used:

$$h_0(t; R; T) = P_{RT}\delta(t - \tau_{RT}) \quad (21)$$

where T and R are the transmitter and receiver elements, P_{RT} is the signal strength received by element R from T, which is calculated according to (6), and τ_{RT} is the signal delay between the two elements, calculated according to

$$\tau_{RT} = \frac{D_{RT}}{c} \quad (22)$$

where c is the speed of light. The second function is used to calculate the impulse response to the signal emitted from an element l, rebounded off an element g and received by an element n and has the form

$$h_r(t; l; g; n) = P_{ngl}\delta(t - \tau_{ng}) \quad (23)$$

where P_{ngl} is calculated according to (10). The impulse response due to each rebound $h_k(t)$, where k represents the number of rebound, is calculated as

$$h_1(t) = \sum_{g=1}^{N}\left[h_0(t; T; g) * h_r(t - \tau_{gT}; T, g, R)\right] \quad (24)$$

$$h_2(t) = \sum_{g=1}^{N}\left[h_0(t; T; g) * \sum_{n=1}^{N}\left(h_r(t - \tau_{gT}; T; g; n) * h_r(t - \tau_{ng} - \tau_{gT}; g; n; R)\right)\right] \quad (25)$$

$$h_3(t) = \sum_{g=1}^{N}\left[h_0(t; T; g) * \sum_{n=1}^{N}\left[h_r(t - \tau_{gT}; T; g; n) * \sum_{l=1}^{N}\left[h_r(t - \tau_{ng} - \tau_{gT}; g; n; l) * h_r(t - \tau_{ln} - \tau_{ng} - \tau_{gT}; n; l; r)\right]\right]\right]. \quad (26)$$

Here, the response is obtained to the impulse from the source element to each g element and is convolved

with the response to the impulse obtained when it is emitted by the source, rebounded off element g, and received at the receiver, delayed by time τ_{gT} due to the distance between the source and the element g. N is the total number of elements forming the environment.

To obtain the total impulse response of all the reflections, from $k = 0$ which represents the LOS path and the other rebounds (from the ground, walls, and ceiling) $k = K$, we generated a recursive function, following (20). The detector receives a sinusoidal signal of the same frequency as the transmitted signal, but with a different amplitude and phase, represented by its phasor according to [30]

$$s = \Re(s) + j\Im(s) \tag{27}$$

where $\Re(s)$ and $\Im(s)$ are the real and imaginary part of s, respectively, and they can be obtained from the impulse response h

$$\Re(s) = \sum_{i=0}^{N} h[i]\cos(\delta[i]) \tag{28}$$

$$\Im(s) = \sum_{i=0}^{N} h[i]\sin(\delta[i]) \tag{29}$$

where

$$\delta[i] = \frac{2\pi t[i]}{T} \tag{30}$$

$$t[i] = iT_s \tag{31}$$

where T is the period of the signal and T_s is the sampling period and phase are given by

$$s = P_s \angle \delta_s \tag{32}$$

where P_s is the amplitude obtained from modulus of the complex number s

$$P_s = \sqrt{\Re(s)^2 + \Im(s)^2} \tag{33}$$

and the phase δ_s

$$\delta_s = \arctan\frac{\Im(s)}{\Re(s)}. \tag{34}$$

The received signal captured by the detector is

$$s(t) = kP_s \sin(2\pi f t + \delta_s). \tag{35}$$

B. Time Dispersion Parameters for the Channel

By using the derived CIR given by (20), we can calculate several channel parameters such as channel dc gain and rms delay spread.

1) Channel DC Gain: Using the calculated CIR, it is possible to analyze or simulate the effect of the wireless optical channel on the performance of VVLC systems. Channel dc Gain using optical link is given by [31]

$$H(0) = \int_{-\infty}^{+\infty} h(t)\mathrm{d}t. \tag{36}$$

The channel gain in dB is given as

$$\text{Channel gain(dB)} = -\log_{10} H(0). \tag{37}$$

2) Channel rms Delay Spread: The received signal, affected by multipath reflection, manifests as a cumulative effect of various weighted and time-delayed versions of the originally transmitted signal. Consequently, the wireless optical multipath channel extends the duration of the transmitted signal, leading to a phenomenon known as temporal dispersion. This key attribute can be measured using the rms delay spread, denoted as τ_{rms}, based on the CIR $h(t)$

$$\tau_{\text{rms}} = \sqrt{\frac{\int_0^\infty (t-\bar{\tau})h^2(t)}{\int_0^\infty h^2(t)}}. \tag{38}$$

A measure of dispersion is provided by RMS-DS defined as the second moment of the impulse response and is given by [31]. Where τ is the mean excess delay and it is given by

$$\bar{\tau} = \frac{\int_0^\infty t h^2(dt)}{\int_0^\infty h^2(t)} = \frac{\sum_i t_i^n h_i^2}{\sum_i h_i^2} = \frac{\sum_{i=0}^{k-1}(i \times T_s)^n h_i^2}{\sum_{i=0}^{k-1} h_i^2} \tag{39}$$

where h_i is the amplitude of the impulse response at time equal to $(n \times Ts)$, it represents the discrete function of $h(t)$. Since delay takes on a very small value, it is expressed as an integer multiple of sampling time. The value of is chosen to be equal to the time it takes light to travel between two neighboring elements [32].

V. Simulation and Results

This section introduces the evaluation setup, equipment used to obtain the results and the time consumed by emulations to evaluate the communication behavior in unfavorable scenarios, according to the proposed model. The evaluation setup is divided into two parts. First, we describe the methodology and the tools used, then the layout of the scenario and the parameters are introduced.

A. Evaluation Methodology

Fig. 6 illustrates the mean steps deployed in this work for channel modeling. First, we include the main system parameters for the environment and tunnel dimensions according to Table I, and the transmitter specifications (i.e., position, orientation, optical power, and radiation pattern) as well as the detector specifications (i.e., detector type (PSD sensor), orientation, aperture size, and field-of-view angle). After data assimilation, a recursive algorithm is used in the simulation tool to determine the signal strength for each reflection (It should be noted that when working with the sensor, the signal arrives instantaneously and the computation of signals from the receiver is done continuously without recursive algorithms; recursive methods are used only in the simulation tool).

The resulting dataset is then ported to MATLAB, facilitating in-depth analysis to investigate the key performance metrics. All computations are performed on a desktop computer with the configuration of AMD Ryzen 5 5600G 3.90 GHz CPU and 16.0 GB RAM.

B. Coverage Modeling

The synthetic environment that has been used to carry out the characterizations is a rectangular tunnel composed

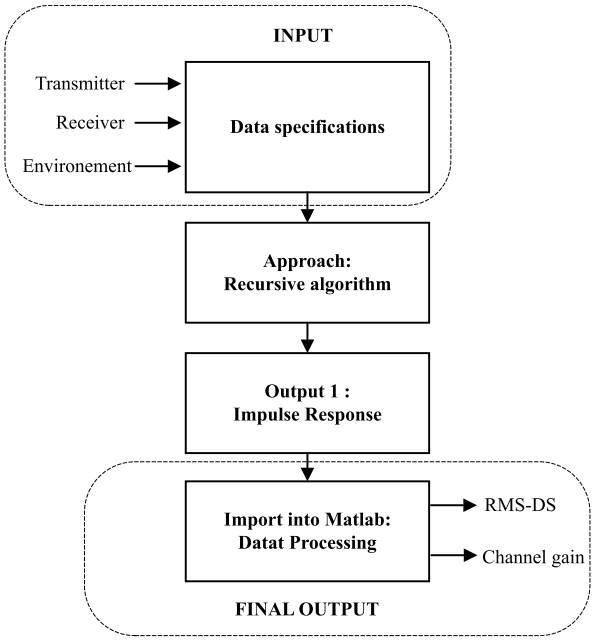

Fig. 6. Main steps of our channel modeling approach.

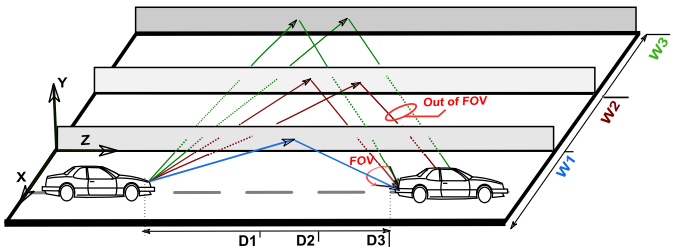

Fig. 7. Overview of the three different scenarios.

of walls, floor, and ceiling. Table I presents the parameters of the V2V communication scenario on a single-lane road, with the source vehicle Tx communicating with the destination vehicle Rx (Fig. 4). We have explored three scenarios, each with varying intervehicular distances (Di), both Tx and Rx are centrally aligned according to scenario A positions. The tunnel dimensions for each scenario considered throughout the article are based in the Spanish national regulation [33], those values can be easily changed in the developed simulator. A material with a strong specular component was chosen for the road, a material between specular and diffuse for the sides, and an almost diffuse material for the roof.

It is worth noting that the run time is influenced by two primary factors: the total number of elements the environment is divided into, and the number of reflections considered. The relationship is represented as N^k, where N signifies the total elements and k is the number of rebounds considered reflections. For example, in scenario B, for a distance of 35 m. The computation times for each rebound are as follows: the first rebounds take 3 s, the second rebounds take 14 433 s (04 h 33 s), and the third take 67 607 s (18 h 46 min 47 s). Consequently, the overall runtime can be expressed as

$$t_{\text{RUN}} \propto \sum_{K=0}^{N} N^k. \tag{40}$$

TABLE I
SCENARIO PARAMETERS

Scenario	Width	Height	Length to evaluate the scenario
Scenario A	W1 = 4.7 m	5 m	D = 15 m, 25 m, 35 m
Scenario B	W2 = 8.5 m	5 m	D = 15 m, 25 m, 35 m
Scenario C	W3 = 11.5 m	5 m	D = 15 m, 25 m, 35 m
Normal vector	$\vec{n}_T = \{0, 0, 1\}$ $\vec{n}_R = \{0, 0, -1\}$		
Position	Tx: {1.55, 0.8, 0}; Rx: {2.35, 0.8, D}		
Vehicle Size	$1.6 \times 4.7 \times 2\ m^3$		
PSD FOV	45°		

It is important to note that the smaller the cell size, the closer the emulated behavior is to real behavior, which would imply a significant simulation time. However, the larger the cell size will reduce the simulation time, but then, the results will become less realistic. To perform the simulations, the following sizes were chosen to divide the surfaces into cells. As a compromise between accuracy and computational time, sizes of 2 cm were chosen to evaluate the first bounce, 10 cm for the second bounce, and 50 cm for the third bounce.

This has been done because the first ones are faster to compute and provide more information, obtaining with these sizes results very similar to the real case. The third bounce, which already arrives with low power and provides less information (known from previous experience [27]), was analyzed with a large cell to avoid the simulation taking weeks. Even the size considered for the second bounce has made it slow to compute, but it has become convenient given the information it provides. The proposed model uses a one-lane tunnel According to Standard 3.1-IC Road Tunnels, following the regulations provided in [32].

1) *Scenario A:* Conventional roads N-332, with a road width of 4.7 m approximately.
2) *Scenario B:* Conventional roads C-40 with 3-m lanes 0.50 m (left-hand width) + 2 lanes of 3.0 m + 0.50 (right-hand width) m + 0.75 × 2 (maintenance lane) = 8.5 m.
3) *Scenario C:* Conventional roads C-100 and C-80.
4) Roadside 1.0 m + lane 3.5 m + intermediate zone 1.0 m + lane 3.5 m + Roadside 1.0 m + 0.75 × 2 = 11.5 m. Seventy-five centimeter (75 cm) wide raised sidewalks will be provided on both sides.

Fig. 7 shows an overview of the three different scenarios, where $w1$, $w2$, and $w3$ the tunnel width according to each scenario. $D1$, $D2$, and $D3$ are 15, 25, and 35 m, respectively. It should be noted that the floor, ceiling, and right wall also exhibit reflections, they are not depicted here to simplify the illustration.

C. Channel Impulse CIR Analysis

The CIR can be evaluated using the channel simulation setup described in Section VI. The following convention will be used: $h0$ is the impulse response for the LOS signal; $h1$, $h2$, and $h3$ are the corresponding impulse responses for first bounce, second bounce, and third bounce. The CIR can be obtained by applying (23)–(25), respectively.

Fig. 8 shows the simulation results obtained during multipath evaluation using our proposed model Fig. 8(a), and Lambertian reflector model Fig. 8(b), as the vehicle passes

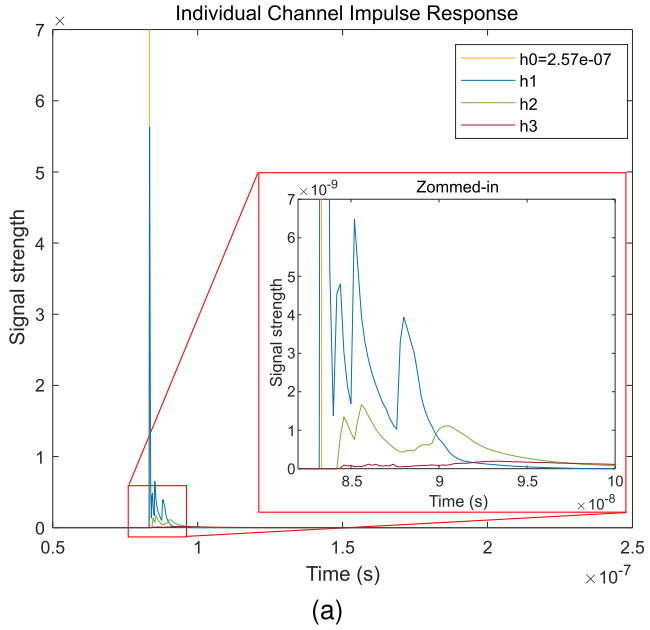

Fig. 8. CIR (using scenario A $D2 = 25$ m). (a) Our model. (b) Lambertian model.

through the tunnel. Here, we consider scenario A at $D2 = 25$ m the intervehicular distance. We selected this scenario to rigorously test the system under a worst-case condition, aiming to understand its resilience and robustness in challenging environments.

The results show that the first reflection in the proposed model has a RSS of $h1 = 5.63e^{-08}$, while in the Lambertian model, it is $h1 = 9.4e^{-10}$. This indicates that the first reflection is much stronger in the proposed model compared to the Lambertian model.

As illustrated in the figures, the RSS is presented in normalized units, relative to the emitted signal strength. The first peak in the CIR of our proposed model is mainly from the ground. Given that the transmitter and receiver are located relatively close to the ground at a height of 0.8 m from the ground, direct reflection from ground surfaces becomes a dominant

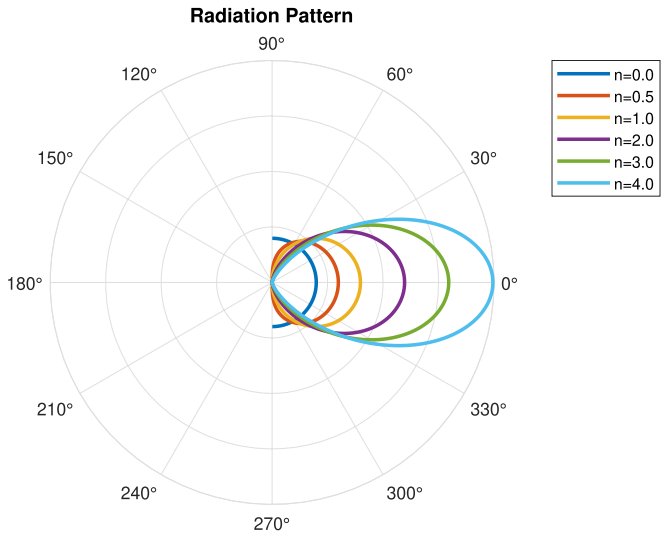

Fig. 9. Radiation emission patterns for different n-index values.

path for the signal. This grounds reflection, combined with the properties of specular reflection, produces a strong, concentrated initial signal. This can be explained with the help of Fig. 5. In contrast, the Lambertian model, based on diffuse reflection, disperses energy more uniformly, resulting in wider, less intense peaks.

On the other hand, in terms of second rebounds ($h2$ components), the proposed model has three distinct peaks, suggesting multiple specific reflection paths due to the combined specular and diffuse reflection pattern.

Conversely, the single pronounced peak of Lambertian model, based only on diffused reflection, highlights a more uniform interaction with the environment. This distinction underlines the nuanced interactions between the paths captured by the proposed model and the average behavior presented by Lambertian model, compared with an almost diffuse approach. It can be observed that the CIR from $h3$ is significantly lower as compared to $h1$ and $h2$, for both models. This is due to two main factors as follows.

1) *Angular Spread and Receiver Field of View:* The receiver has Reflections that occur outside this angular range may not be captured effectively, resulting in reduced signal intensity for these reflections.
2) *Path Loss:* With each successive reflection, the light must travel a greater distance before reaching the receiver. Each time the signal reflects off a surface, some of its energy is lost through absorption, scattering or diffraction. By the third reflection, the signal has traveled a much longer path and interacted with the surfaces several times, resulting in increased attenuation.

D. Effect of Focal Length and Lambertian Order of the Emitter Diagram on CIR Using Our Proposed Model

In this section, we analyze the impact of focal length and Lambertian order of the emitter diagram variations on the CIR using our proposed model. Figs. 9–13 show the impulse responses characterized by signal strength as a function of time for different configurations of Lambertian order ($n1 = 1$, $n2 = 3$), and focal lengths ($f1 = 4.5$ mm, $f2 = 8$ mm, and

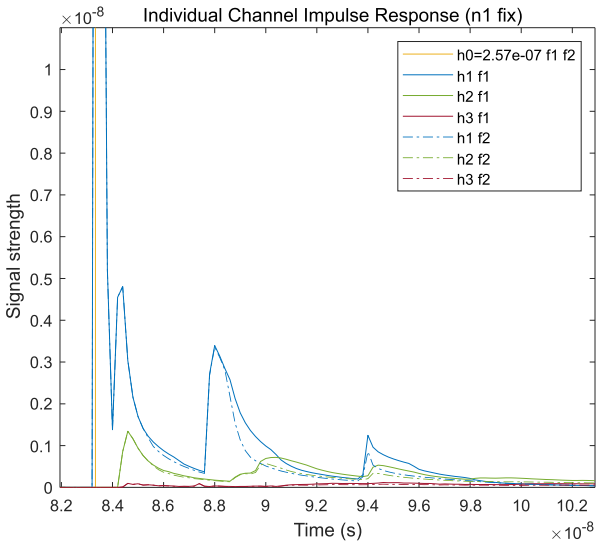

Fig. 10. CIR (using scenario A, $D2 = 25$ m, $f1 = 4.5$ mm, $f2 = 8$ mm, fixed $n1 = 1$).

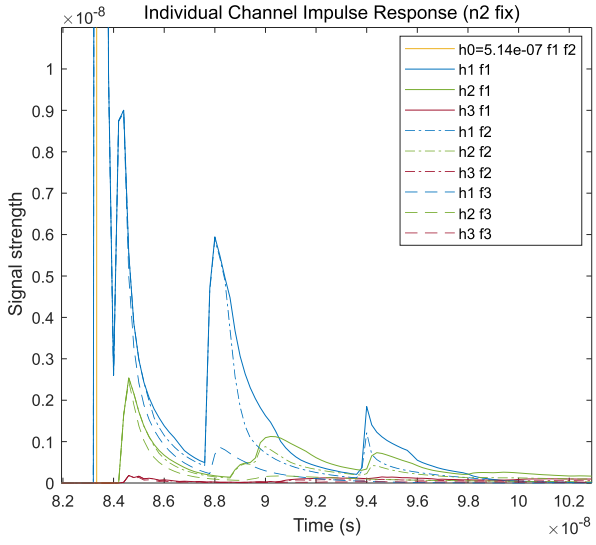

Fig. 11. CIR (using scenario A $D2 = 25$ m, for $f1 = 4.5$ mm, $f2 = 8$ mm, $f3 = 16$ mm, fixed $n2 = 3$).

$f3 = 16$ mm). In Fig. 9, we present several emission patterns as a function of Lambertian order n.

Fig. 10 illustrates how the impulse response varies with the focal length assuming a constant Lambertian order (with $n1 = 1$). We analyze the impact of varying different focal lengths on the CIR. It can be observed that with focal length $f2$ (greater focal length), the effects of multipaths are smaller than with focal length $f1$. This effect can be seen more clearly in the impulse response due to the first reflection $h1$. This is because increasing the focal distance narrows the receiver's FoV, resulting in less wall, floor or ceiling within the receiver's FoV, thus receiving fewer multipath signals.

Fig. 11 shows the impulse responses (CIR) for a Lambertian order fixed at $n2 = 3$, Comparing Fig. 11, which uses a Lambertian order $n2 = 3$, with the Fig. 10, where $n = 1$, we observe significant differences in the distribution and intensity of VLC signals. The higher Lambertian order in Fig. 11 leads to a more directional transmission of light, which is manifested by a more concentrated and potentially stronger intensity of the LOS signal ($h0 = 5.14$e-07). With a longer focal length $f3 = 16$ mm, the light will be more focused and directional, which can improve direct LOS signal quality but can also reduce the coverage and the multipath effect. This can be seen in Fig. 11, by the reduction in reflection signals ($h1$, $h2$, $h3$) for $f3$ compared with $f1$ and $f2$.

Fig. 12 shows the results for the two distinct Lambertian orders, $n1$ and $n2$, with a fixed focal length $f1$. It can be seen that the lower Lambertian order, $n1 = 1$, indicates a more extensive and uniform light distribution. In contrast, the higher Lambertian order, $n2 = 3$, reflects a more directional light transmission, offering stronger signal intensity in direct LOS.

Fig. 13 shows the total channel impulse and compares six different configurations combining two Lambertian orders ($n1$ and $n2$) with three different focal lengths ($f1$, $f2$, $f3$). The differences between the curves for each focal length ($f1$, $f2$, $f3$) in the same Lambertian orders indicate the impact of focal length on range and signal intensity.

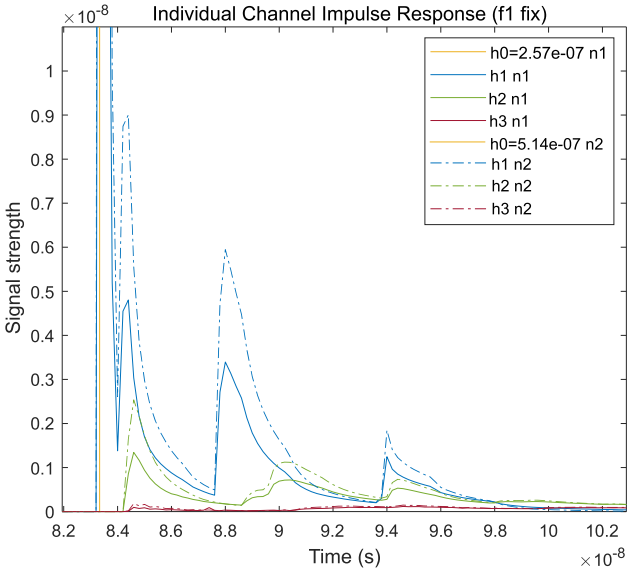

Fig. 12. CIR (using scenario A $D2 = 25$ m, for $n1 = 1$, $n2 = 3$, fixed $f1 = 4.5$ mm).

After analyzing the results shown in Figs. 10–13, it can be concluded that the greater the focal length or the higher the index n of the emission pattern, the lesser the multipath effect. This is because as the focal length increases, the FoV decreases, resulting in fewer surfaces within the receiver's FoV, leading to a reduced reception of multipath signals. Similarly, increasing the value of the Lambertian order of the emission pattern (n) results in a more directional emission, delivering more power to the receiver and less to the surfaces. Consequently, the multipath effect diminishes.

E. Effect of Intervehicular Spacing on CIR

Fig. 14 shows the influence of intervehicular spacing on the CIR, with the V2V distance placed at a distance of 15, 25, and 35 m on the Z axis. The analysis of the CIR reveals a noticeable trend toward decreasing amplitude with increasing distance. As the distance between vehicles increases from 15 to 35 m, the CIR decreases from 1.721e-7 at 15 m

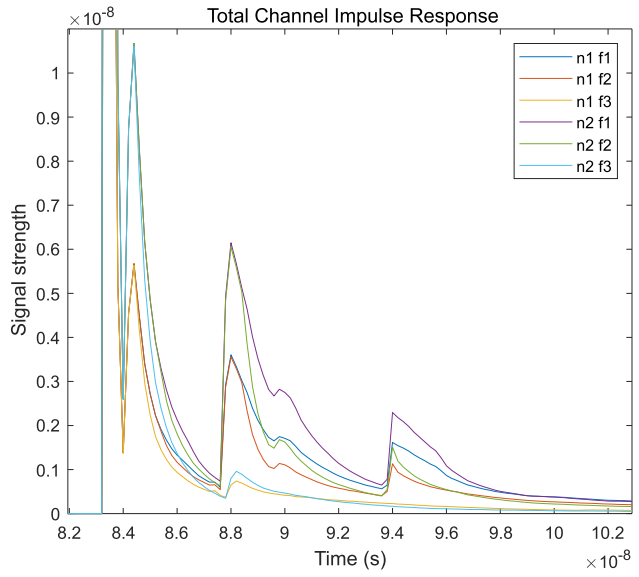

Fig. 13. Total CIR (using scenario A, $D2 = 25$ m, for $n1 = 1$, $n2 = 3$).

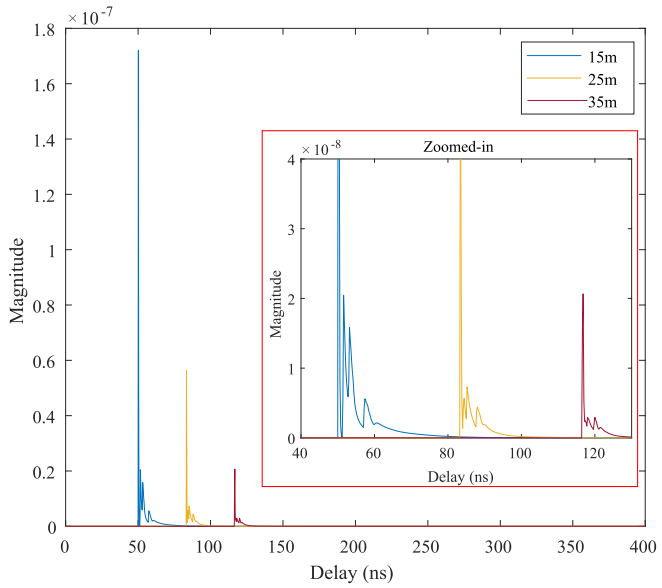

Fig. 14. Channel multipath CIR versus delay for different distances scenario A.

to 0.206e-7 at 35 m, reflecting the cumulative effects of LOS loss-of-trajectory and NLOS interactions. The corresponding delay also increases, indicating a more complex multipath environment at greater distances.

Specifically, the dominance of direct LOS signals is evident at short distances, while at longer distances, NLOS influences, including specular and diffuse reflections, become prominent, resulting in greater delay and reduced signal strength. Table II presents the RMS-DS values obtained for the two models: the proposed model and the Lambertian model, considering the three different scenarios (Table I). As can be seen, the Lambertian reflector model, which is based on ideal diffuse reflections, seems to predict a more dispersed multipath environment, resulting in a higher rms delay. This model generally assumes that reflected waves are uniformly scattered in all directions, leading to a wide range of arrival times for multipath components, resulting in greater delay dispersion (Table II).

TABLE II
SIMULATIONS RESULTS OF RMS-DS

		RMS Delay (ns)	
	Distance	Proposed model	Lambertian Model
Scenario A	15 m	1.19 ns	5.30 ns
	25 m	1.25 ns	4.79 ns
	35 m	1.24 ns	4.78 ns
Scenario B	15m	1.17 ns	7.41 ns
	25 m	1.46 ns	7.42 ns
	35 m	1.76 ns	6.33 ns
Scenario C	15m	0.93 ns	4.78 ns
	25 m	1.34 ns	9.07 ns
	35 m	1.63 ns	8.90 ns

F. Impact of Tunnel Width and Intervehicular Distance

The purpose of the analysis is to understand the dependence of the CIR and RMS-DS on two key parameters: distance and tunnel width. From Fig. 15, and using Table II, we can clearly see that for the different widths, the RMS-DS values show a distinctive pattern. At a distance of 15 m inside the tunnel, the RMS-DS delay spread is lowest for the widest dimension of the tunnel (11 m), at 0.93 ns.

As the tunnel narrows, this value increases slightly to 1.17 ns for a width of 8.5 m, and intensifies further to 1.19 ns for a width of 4.7 m. When we move on to a distance of 25 m, the RMS-DS measurements illustrate a more mixed behavior: the widest dimension of the tunnel (11 m) registers 1.34 ns, while the narrower widths of 8.5 and 4.5 m register values of 1.46 and 1.25 ns, respectively. At the furthest distance of 35 m, RMS-DS values are 1.63, 1.76, and 1.24 ns for tunnel widths of 11, 8, and 4 m, respectively. The results demonstrate a significant interaction between tunnel width, propagation distance and the resulting multipath effects. Given the centralized positioning of transmitter and receiver within a 4.7 m width, wider tunnels can lead to additional reflections and scattering phenomena, which are then picked up differently by the receiver's FoV. This can be explained with the help of Fig. 7. The limited FOV of the receiver can influence the multipath components received. Signals reflected outside this FOV will not be detected by the receiver.

This is why:

1) *Tunnel Width and PSD's FOV:* A wider tunnel may cause some multipath components to be reflected outside the FOV, particularly for Tx and Rx positioned toward scenario A (Fig. 7). This may explain why, in some cases, the RMS-DS is lower for wider tunnels.
2) *Distance and PSD's FOV:* As distance increases, the angular dispersion of multipath components can also increase. In a limited FoV, this can lead to the receiver capturing fewer multipath components, which influences the RMS-DS.

Fig. 16, which represent the CIR provide a comprehensive view of the signal propagation characteristics in different tunnel scenarios. The CIR values underscore the dominance of the direct and reflected paths, which vary based on tunnel width and distance. A 4.7 m width offers the strongest signal convergence, especially when the transmitter and receiver are centralized. However, as the width increases, the RSS decreases, indicating that reflected paths are longer and perhaps less constructive.

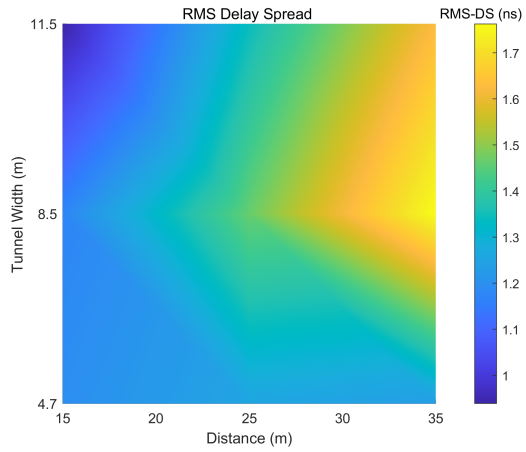

Fig. 15. RMS delay spread versus intervehicular distance and tunnel width.

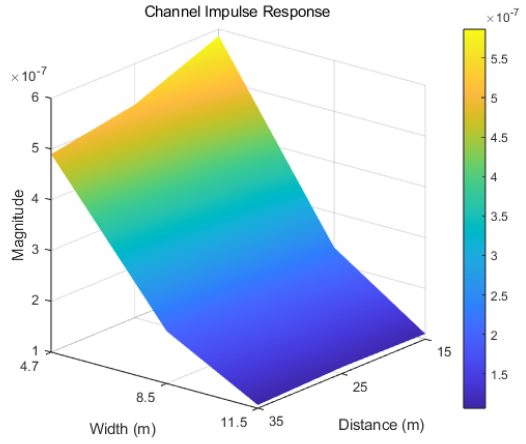

Fig. 16. CIR distribution versus intervehicular distance and tunnel width.

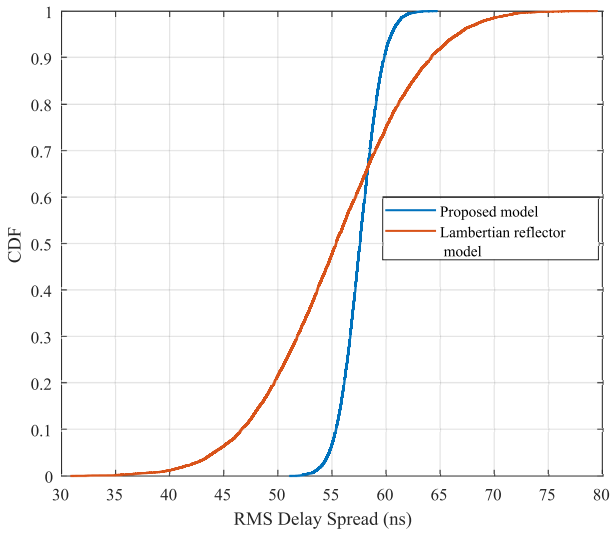

Fig. 17. CDF of rms delay Spread considering scenario A, with $D = 25$ m.

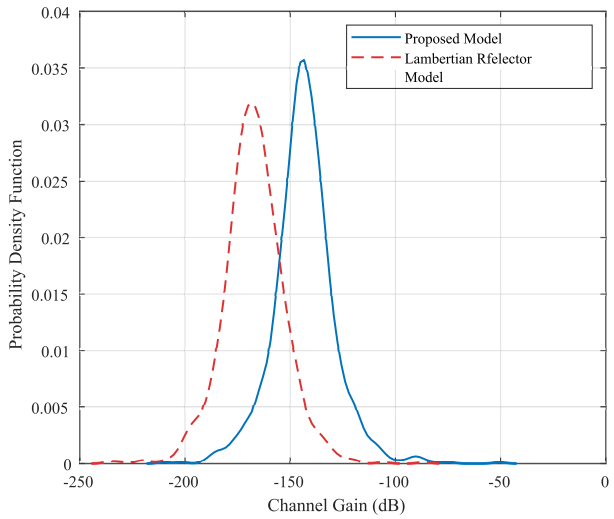

Fig. 18. PDF of channel gain of the reflection component of the VVLC path loss (excluding LOS path gain), considering scenario A when $D = 25$ m.

G. Statistical Metrics Analysis

In Figs. 17 and 18, we present the results of a Monte Carlo simulation designed to provide a comprehensive understanding of channel behavior by analyzing the cumulative distribution function (cdf) of rms delay and the probability density function (pdf) of channel gain. By conducting Monte Carlo simulations with a Gaussian input and analyzing the resultant cdf, we aim to capture a broader view of the behavior of channel. This offers insights into how the system might behave under varied real-world input conditions. We have compared our proposed model with diffuse models according to scenario A with an intervehicular distance of 25 m. This simulation was conducted using a Monte Carlo approach with 103 iterations. In Fig. 17, the proposed model, which includes both specular and diffuse reflections, shows a rms delay spread ranging from 50.57 to 68.86 ns. In contrast, the Lambertian model, based on diffuse reflections only, showed a wider range, from 31.30 to 78.66 ns. A noticeable intersection at 58.26 ns, corresponding to a cdf of 0.65, implies that for around 65% of cases, the two models give similar views of the channel up to this delay gap. Beyond this point, the two models diverge significantly. The proposed model begins with a larger delay, which can theoretically be associated with the presence of specular reflections.

These reflections, being deterministic, can lead to certain signal paths having a significant delay, manifesting as a peak in the impulse response. As the delay increases and diffuse components become more influential (since all signals exhibit some level of scattering), the behaviors of the two models converge. This is evident in the intersection point mentioned. This convergence could be due to the randomness of diffuse reflections dominating the behavior of both models after a specific period. In Fig. 18, the proposed model provides a more robust gain range from -75.24 to -207 dB.

The average attenuation is -145.1 dB, with the concentration of channel gains, as shown in the pdf peak, at 0.036. In contrast, (purely diffuse reflections) extends over a wider attenuation spectrum, from -101 to -273 dB. Its mean value rises to -167.5 dB, and its pdf peak distribution falls slightly to 0.030. As specular reflections are deterministic, they retain greater signal strength, giving the proposed model its significant gains. On the other hand, the more attenuated nature

of Lambertian model is indicative of the random scattering associated with purely diffuse reflections, resulting in greater signal dispersion and, consequently, weaker received signals.

Furthermore, in a such confined environment where the main focus is on multipath components (excluding LOS), the fusion of specular and diffuse reflections in the proposed model results in more stable and predictable channel behavior. This can be particularly beneficial in environments with a combination of reflective surfaces, ensuring reliable communication despite the absence of a direct line of sight. In contrast, Lambertian model, by relying entirely on diffuse reflections, highlights the difficulties and potential unreliability of VLC in spaces where these reflections dominate, particularly in the absence of a direct line of sight.

VI. Conclusion

In this article, we have presented a novel multipath channel model and the behavior of a PSD-based sensor for V2V VLC in a rectangular-shaped tunnel environment. Moreover, the statistical characteristics and analytical results of the proposed model provide insight into the real tunnel propagation environment for VLC. The discrepancy between the rms delay values of the proposed model and Lambertian model underlines the importance of model selection in accurately characterizing vehicular channels. It indicates that the specific characteristics of the environment and the nature of the reflections have a significant influence on the characteristics of multipath propagation, affecting delay spread and, consequently, overall system performance. The distinct behaviors of the two models highlight the importance of considering all reflection types. The proposed model, capturing both reflection types, offers a more comprehensive view of the system, essential for real-world applications where both reflection types are always in play.

From the analysis and quantification of the multipath effect using the proposed model, we can conclude that the proposed model based on a discretized approach suggests that VLC has the potential to be a robust technology for V2V in closed environments, even without a direct line of sight. This could enable more reliable communications in situations where vehicles are in motion and LOS is often obstructed.

Author Contributions

Conceptualization: José-Luis Lázaro-Galilea, Alfredo Gardel-Vicente, Abdeljabbar Cherkaoui; data curation: Fatima Zahra Raissouni, Álvaro De-La-Llana-Calvo; formal analysis: Álvaro De-La-Llana-Calvo, José-Luis Lázaro-Galilea; funding acquisition: Alfredo Gardel-Vicente, José-Luis Lázaro-Galilea, Abdeljabbar Cherkaoui; investigation: Fatima Zahra Raissouni, José-Luis Lázaro-Galilea, Alfredo Gardel-Vicente, Álvaro De-La-Llana-Calvo, Abdeljabbar Cherkaoui; methodology: José-Luis Lázaro-Galilea, Álvaro De-La-Llana-Calvo; project administration: Álvaro De-La-Llana-Calvo, José-Luis Lázaro-Galilea, Alfredo Gardel-Vicente; resources: José-Luis Lázaro-Galilea, Álvaro De-La-Llana-Calvo; software: Fatima Zahra Raissouni, Álvaro De-La-Llana-Calvo; supervision: José-Luis Lázaro-Galilea; validation: Fatima Zahra Raissouni, Álvaro De-La-Llana-Calvo, Alfredo Gardel-Vicente, José-Luis Lázaro-Galilea; visualization: Álvaro De-La-Llana-Calvo, José-Luis Lázaro-Galilea; writing—original draft: Fatima Zahra Raissouni; and writing—review and editing: Fatima Zahra Raissouni, José-Luis Lázaro-Galilea, Alfredo Gardel-Vicente, Álvaro De-La-Llana-Calvo, Abdeljabbar Cherkaoui. All authors read and agreed to the published version of the paper.

Acknowledgment

Fatima Zahra Raissouni thanks “María de Guzmán” Residence and Collaboration Scholarship Programs of the University of Alcalá (UAH) for Cotutelle Ph.D. Program.

References

[1] P. K. Singh, S. K. Nandi, and S. Nandi, “A tutorial survey on vehicular communication state of the art, and future research directions,” *Veh. Commun.*, vol. 18, Aug. 2019, Art. no. 100164. [Online]. Available: https://www.sciencedirect.com/science/article/pii/S2214209618300901

[2] *IEEE Standard for Information Technology-Local and Metropolitan Area Networks-Specific Requirements—Part 11: Wireless LAN Medium Access Control (MAC) and Physical Layer (PHY) Specifications Amendment 6: Wireless Access in Vehicular Environments*, Standard IEEE 802, IEEE Piscataway, NJ, USA, 2010.

[3] V. Vukadinovic et al., “3GPP C-V2X and IEEE 802.11p for vehicle-to-vehicle communications in highway platooning scenarios,” *Ad Hoc Netw.*, vol. 74, pp. 17–29, Jan. 2018. [Online]. Available: https://www.sciencedirect.com/science/article/pii/S157087051830057X

[4] S. Caputo, L. Mucchi, M. A. Umair, M. Meucci, M. Seminara, and J. Catani, “The role of bidirectional VLC systems in low-latency 6G vehicular networks and comparison with IEEE802.11p and LTE/5G C-V2X,” *Sensors*, vol. 22, no. 22, p. 8618, Nov. 2022. [Online]. Available: https://www.mdpi.com/1424-8220/22/22/8618

[5] A.-M. Cailean and M. Dimian, “Impact of IEEE 802.15.7 standard on visible light communications usage in automotive applications,” *IEEE Commun. Mag.*, vol. 55, no. 4, pp. 169–175, Apr. 2017. [Online]. Available: https://ieeexplore.ieee.org/abstract/document/7901496

[6] L. Bernado et al., “In-tunnel vehicular radio channel characterization,” in *Proc. IEEE 73rd Vehicular Technol. Conf.*, May 2011, pp. 1–5. [Online]. Available: https://ieeexplore.ieee.org/abstract/document/5956510

[7] M. Yusuf et al., “Experimental investigation of V2I radio channel in an arched tunnel,” in *Proc. 13th Eur. Conf. Antennas Propag. (EuCAP)*, Mar. 2019, pp. 1–5. [Online]. Available: https://ieeexplore.ieee.org/abstract/document/8739526

[8] N. Avazov, S. M. R. Islam, D. Park, and K. S. Kwak, “Statistical characterization of a 3-D propagation model for V2V channels in rectangular tunnels,” *IEEE Antennas Wireless Propag. Lett.*, vol. 16, pp. 2392–2395, 2017. [Online]. Available: https://ieeexplore.ieee.org/abstract/document/7959179

[9] W.-H. Shen and H.-M. Tsai, “Testing vehicle-to-vehicle visible light communications in real-world driving scenarios,” in *Proc. IEEE Veh. Netw. Conf. (VNC)*, Nov. 2017, pp. 187–194. [Online]. Available: http://ieeexplore.ieee.org/document/8275596/

[10] Á. De-La-Llana-Calvo, J.-L. Lázaro-Galilea, A. Gardel-Vicente, D. Rodríguez-Navarro, B. Rubiano-Muriel, and I. Bravo-Muñoz, “Analysis of multiple-access discrimination techniques for the development of a PSD-based VLP system,” *Sensors*, vol. 20, no. 6, p. 1717, Mar. 2020.

[11] Z. Cui, C. Wang, and H.-M. Tsai, “Characterizing channel fading in vehicular visible light communications with video data,” in *Proc. IEEE Veh. Netw. Conf. (VNC)*, Dec. 2014, pp. 226–229. [Online]. Available: https://ieeexplore.ieee.org/abstract/document/7013353

[12] L.-C. Wu and H.-M. Tsai, “Modeling vehicle-to-vehicle visible light communication link duration with empirical data,” in *Proc. IEEE Globecom Workshops (GC Wkshps)*, Dec. 2013, pp. 1103–1109. [Online]. Available: https://ieeexplore.ieee.org/abstract/document/6825140

[13] T. Nawaz, M. Seminara, S. Caputo, L. Mucchi, and J. Catani, “Low-latency VLC system with Fresnel receiver for I2 V ITS applications,” *J. Sensor Actuator Netw.*, vol. 9, no. 3, p. 35, Jul. 2020. [Online]. Available: https://www.mdpi.com/2224-2708/9/3/35

[14] F. Z. Raissouni and A. Cherkaoui, “A geometry-based analytical model for vehicular visible light communication channels,” in *Proc. Int. Conf. Adv. Intell. Syst. Sustain. Develop.* (Lecture Notes in Networks and Systems), J. Kacprzyk, M. Ezziyyani, and V. E. Balas, Eds. Cham, Switzerland: Springer, 2023, pp. 64–72.

[15] M. Karbalayghareh et al., "Channel modelling and performance limits of vehicular visible light communication systems," *IEEE Trans. Veh. Technol.*, vol. 69, no. 7, pp. 6891–6901, Jul. 2020.

[16] P. Luo, Z. Ghassemlooy, H. L. Minh, E. Bentley, A. Burton, and X. Tang, "Performance analysis of a car-to-car visible light communication system," *Appl. Opt.*, vol. 54, no. 7, p. 1696, Mar. 2015. [Online]. Available: https://www.osapublishing.org/abstract.cfm?URI=ao-54-7-1696

[17] F. Z. Raissouni, A. Cherkaoui, J. L. L. Galilea, and A. Gardel Vicente, "Performance metrics for vehicular visible light communication systems," in *Proc. ITM Web Conf.*, vol. 48, Jan. 2022, p. 01014. [Online]. Available: https://www.itm-conferences.org/articles/itmconf/abs/2022/08/itmconf_iccwcs2022_01014/itmconf_iccwcs2022_01014.html

[18] M. Uysal, Z. Ghassemlooy, A. Bekkali, A. Kadri, and H. Menouar, "Visible light communication for vehicular networking: Performance study of a V2V system using a measured headlamp beam pattern model," *IEEE Veh. Technol. Mag.*, vol. 10, no. 4, pp. 45–53, Dec. 2015.

[19] M. Meucci, M. Seminara, T. Nawaz, S. Caputo, L. Mucchi, and J. Catani, "Bidirectional vehicle-to-vehicle communication system based on VLC: Outdoor tests and performance analysis," *IEEE Trans. Intell. Transp. Syst.*, vol. 23, no. 8, pp. 11465–11475, Aug. 2022.

[20] D. Iturralde, C. Azurdia-Meza, N. Krommenacker, I. Soto, Z. Ghassemlooy, and N. Becerra, "A new location system for an underground mining environment using visible light communications," in *Proc. 9th Int. Symp. Commun. Syst., Netw. Digit. Sign (CSNDSP)*, Jul. 2014, pp. 1165–1169. [Online]. Available: https://ieeexplore.ieee.org/abstract/document/6924006

[21] D. Iturralde, F. Seguel, I. Soto, C. Azurdia, and S. Khan, "A new VLC system for localization in underground mining tunnels," *IEEE Latin Amer. Trans.*, vol. 15, no. 4, pp. 581–587, Apr. 2017. [Online]. Available: https://ieeexplore.ieee.org/abstract/document/7896341

[22] P. P. Játiva et al., "A VLC channel model for underground mining environments with scattering and shadowing," *IEEE Access*, vol. 8, pp. 185445–185464, 2020. [Online]. Available: https://ieeexplore.ieee.org/abstract/document/9222015

[23] J.-H. Lee and S.-Y. Jung, "SNR analyses of the multi-spectral light channels for optical wireless LED communications in intelligent transportation system," in *Proc. IEEE 79th Vehicular Technol. Conf.*, May 2014, pp. 1–5. [Online]. Available: https://ieeexplore.ieee.org/abstract/document/7023099

[24] E. Torres-Zapata, V. Guerra, J. Rabadan, R. Perez-Jimenez, and J. M. Luna-Rivera, "Vehicular communications in tunnels using VLC," in *Proc. 15th Int. Conf. Telecommun.*, Jul. 2019, pp. 1–6. [Online]. Available: https://ieeexplore.ieee.org/abstract/document/8848500

[25] Á. De-La-Llana-Calvo et al., "Modeling the effect of optical signal multipath," *Sensors*, vol. 17, no. 9, p. 2038, Sep. 2017. [Online]. Available: https://www.mdpi.com/1424-8220/17/9/2038

[26] Á. De-La-Llana-Calvo et al., "Modeling infrared signal reflections to characterize indoor multipath propagation," *Sensors*, vol. 17, no. 4, p. 847, Apr. 2017. [Online]. Available: https://www.mdpi.com/1424-8220/17/4/847

[27] Á. De-La-Llana-Calvo, J.-L. Lázaro-Galilea, A. Gardel-Vicente, D. Rodríguez-Navarro, I. Bravo-Muñoz, and F. Espinosa-Zapata, "Characterization of multipath effects in indoor positioning systems by AoA and PoA based on optical signals," *Sensors*, vol. 19, no. 4, p. 917, Feb. 2019. [Online]. Available: https://www.mdpi.com/1424-8220/19/4/917

[28] I. A. Ivan, M. Ardeleanu, G. J. Laurent, N. Tan, and C. Clevy, "The metrology and applications of PSD (position sensitive detector) sensors for microrobotics," in *Proc. Int. Symp. Optomechatronic Technol.*, Oct. 2012, pp. 1–2. [Online]. Available: https://ieeexplore.ieee.org/abstract/document/6403287

[29] Union Nations Economic Commission for Europe Vehicle Regulations. (2013). *United Nations Economic Commission for Europe Vehicle Regulations*. [Online]. Available: https://unece.org/fileadmin/DAM/trans/main/wp29/wp29regs/2013/R112r3e.pdf

[30] H. Fox and W. Bolton, *Mathematics for Engineers and Technologists*. Amsterdam, The Netherlands: Elsevier, Jul. 2002.

[31] Z. Ghassemlooy, W. Popoola, and S. Rajbhandari, *Optical Wireless Communications: System and Channel Modelling With MATLAB*. Boca Raton, FL, USA: CRC Press, Apr. 2019.

[32] J. R. Barry, J. M. Kahn, W. J. Krause, E. A. Lee, and D. G. Messerschmitt, "Simulation of multipath impulse response for indoor wireless optical channels," *IEEE J. Sel. Areas Commun.*, vol. 11, no. 3, pp. 367–379, Apr. 1993. [Online]. Available: https://ieeexplore.ieee.org/abstract/document/219552

[33] DDC Ministerio de Transportes, Movilidad Y Agenda Urbana. (2020). *Norma 3.1-IC. Trazado (Orden FOM/273/2016 de 19 de Febrero de 2016)*. [Online]. Available: https://www.mitma.gob.es/carreteras/normativa-tecnica/06-trazado

Fatima Zahra Raissouni received the M.Sc. degree in mechatronics engineering from the University of Abdelmalek Essaadi, Tetouan, Morocco, in 2019. She is currently pursuing the Ph.D. degree from the University of Alcala (GEINTRA Research Group-EPS), Alcala de Henares, Spain, and the University of Abdelmalek Essaadi (the LTI-Laboratory ENSAT), under a Cotutelle Agreement.

Her current research interests include vehicular communication and positioning using visible light/automotive lighting for intelligent transportation systems.

Álvaro De-La-Llana-Calvo received the Ph.D. degree in electronics from the University of Alcalá, Alcala de Henares, Spain, in 2020.

He currently holds the position of Lecturer at the Department of Electronics, University of Alcalá. His research interests include indoor positioning by infrared and visible light, range sensor fusion, and smart devices.

José-Luis Lázaro-Galilea received the Ph.D. degree in telecommunication engineering from the University of Alcalá, Alcala de Henares, Spain, in 1998.

He currently holds the position of Full Professor at the Department of Electronics, University of Alcalá. His research interests include indoor positioning by infrared and visible light, range sensor fusion, and smart devices.

Alfredo Gardel-Vicente was born in Guadalajara, Spain. He received the Ph.D. degree in telecommunications engineering and computer vision from both the University of Alcala, Alcala de Henares, Spain, and the University of Clermont-Ferrand, Clermont-Ferrand, France, in 2004.

He currently holds the position of Full Professor at the Department of Electronics, University of Alcalá. His primary research interests include programmable hardware/software embedded systems, computer vision, and smart devices.

Abdeljabbar Cherkaoui received the Ph.D. degree in automatic signals and systems from the University of Sidi Mohamed Benabdelah, Fes, Morocco, in 2009.

He currently holds the position of Full Professor at the Department of Electrical and Industrial Engineering, ENSA Tangier, Tangier, Morocco. His research interests include signal processing, image processing, and multiagent architectures adapted to fuzzy classification.